Investigating Single-Molecule Fluorescence Spectral Heterogeneity of Rhodamines Using High-Throughput Single-Molecule Spectroscopy

Yang Zhang,[*, †, £] Yu Zhang,[‡, £] Ki-Hee Song,[†] Wei Lin,[‡] Cheng Sun,[§] George C. Schatz,[‡] Hao F. Zhang[†]

[†] *Departments of Biomedical Engineering,* [§]*Department of Mechanical Engineering, and* [‡]*Department of Chemistry, Northwestern University, Evanston, IL60208, United States*

[*]*E-Mail: yang.zhangfl@gmail.com*

Abstract: We experimentally investigated several intra-molecular coordinate and environmental changes as potential causes of single-molecule fluorescence spectral heterogeneities (smFSH). We developed a high-throughput single-molecule spectroscopy technique to analyze more than 5,000 single-molecule emission spectra from each of nine commonly used fluorophores with different structural rigidities deposited on substrates with different polarities. We observed an unexpected high smFSH from structurally rigid Rhodamine B compared with a structurally flexible Cyanine dye - Alexa Fluor 647. Based on experimentally measured smFSH, we ruled out the system's noise uncertainty, single-molecule spectral diffusion, and environmental polarity as the primary causes of the high smFSH. We found that the rotational flexibility of N, N-dialkylated groups contributed to the smFSH. With the high smFSH observed in structurally more rigid model fluorophores, we speculated that other intra-molecular coordinate and environmental changes might also contribute to the high smFSH in Rhodamines.

TOC Graphic:

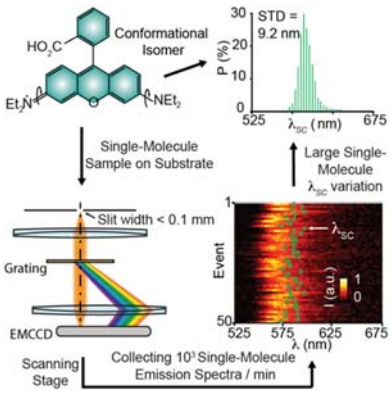

Single-molecule localization microscopy (SMLM) enables nanoscopic imaging of subcellular architectures and dynamics at the molecular level.[1-3] We and others recently developed spectroscopic SMLM (sSMLM) to capture further the full emission spectrum of each individual single-molecule, which is overlooked in conventional SMLM (Figure **1A**).[4-8] Capturing and analyzing unique spectroscopic signatures of individual single-molecule fluorescence, sSMLM permits simultaneous multiplexed super-resolution imaging,[4, 9] detecting nanoscale polarity and hydrophobicity changes,[8, 10-13] and probing multiple reaction pathways[14].

Single-molecule fluorescence spectral heterogeneity (smFSH) refers to the spectral variations of the single-molecule fluorescence emission from the same type of molecules. While this previously could only be observed in single-molecule spectroscopy, smFSH now becomes an integral feature unique to the sSMLM.[5,7,9,13-15] For example, fluorophores with lower smFSH, such as Alexa Fluor 647 (AF647), are favorable for multicolor sSMLM imaging.[4,9] On the other hand, fluorophores with higher smFSH can provide high sensitivity in altering their emission spectrum in responding to local environmental changes[8,10,12-13], a potential benefit towards functional sSMLM imaging.[10] However, despite its promising potential, the root cause of smFSH is yet to be fully understood. The general perception that molecular rigidity is negatively correlated with the smFSH is rather contradictory to experimental observations. For example, the AF647 molecule exhibits low smFSH, but it possesses flexible polymethine bridges that lead to twisted conformations[16]. In turn, high smFSH of Rhodamines, which maintains relatively rigid molecular conformations, has been observed in single-molecule spectroscopy since the 1990s.[17-19] The hypothesis of spectral variations arising from intra-molecular coordinate and environmental changes as the cause of smFSH has been proposed for years.[17] However, the mechanisms of molecular coordinate changes under these conditions that underlie smFSH need to be further investigated. Towards this goal, we aim to decipher the causes of the high smFSH of Rhodamines from common sources of spectral variations as a model system. The abundance of Rhodamine derivatives with distinct molecular structures and well-characterized spectroscopic features makes it an ideal model system for investigating the origin of smFSH.

In this work, we report a method for high-throughput single-molecule spectroscopy (SMS) using sSMLM. By optimizing molecular sparsity and implementing a line scan over the field of view (FOV), we extended the measurement capability to non-blinking fluorophores. [8-14] We used

fluorophores from the Rhodamine family as the model system. The minor differences in the molecular conformation of the individual fluorophores were used to resemble the variation of the intra-molecular coordinate changes. We also used engineering substrates to resemble environmental polarities changes. Experimentally, we collected > 5×10^3 single-molecule emission spectra for each model fluorophore species and performed statistical analyses of the spectral variations among individual single-molecule spectra to quantify smFSH. By correlating the smFSH of these fluorophores with their distinct structural features, we examined possible origins of smFSH in Rhodamines associated with polarity, structural, and conformational changes.

In our sSMLM system[5,9], the single-molecule emission signals were collected using an inverted microscope (Nikon Ti-E) equipped with a 100× total-internal-reflection-fluorescence (TIRF) objective. Then the photons entered a home-built grating-based spectrometer consisting of an entrance slit, a pair of relay lenses, and a transmission grating (Figure **1A**). These photons were split into the 0^{th}- and 1^{st}-order images and concurrently captured by an electron-multiplying charge-coupled device (EMCCD). Finally, the spatial and spectral information of each single-molecule emitter was analyzed from the spatial (0^{th}-order) and spectral (1^{st}-order) images (Figure **1B**). We modified the sSMLM system to enable the high-throughput SMS of non-switchable fluorescent molecules for quantitative analysis of smFSH. Specifically, we adjusted the entrance slit width to < 100 μm to confine the width of the imaging field-of-view (FOV) in the spatial image to be < 0.8 μm (Figure **1C**). Such a strategy has been developed for examining the single-particle photoluminescence spectra of densely packed non-blinking quantum dots.[20-21] Considering the limited photon budget (<5,000 photons) of the investigated fluorophores and the tradeoff between achievable spectral resolution and spectral precision[22], we selected a spectral dispersion of 0.33 pixel/nm for our spectrometer, set a camera exposure time of 50 ms, applied an illumination power of 50-100 W cm^{-2}, and filtered out dim molecules (< 500 photons). The background in the SMS configuration is 3-4 fold lower than the previous imaging configuration to minimize the contribution of the system's noise uncertainty (Figure **S1A**) to offer a spectral precision of 2.5 nm when the photon signal is 500 photon. We also performed numerical simulations of the system's spectral precision at different background levels to exclude the influence of background noise on quantifying smFSH (Figure **S1B**). Under this condition and by scanning the sample stage horizontally, we can capture >5×10^3 of single-molecule spectra within 5 minutes. Compared with scanning the wide FOV provided in the existing Figure **1B**'s configuration, the point density[23] of

single molecules can be, in principle, increased by 100-fold to reduce the scanning time (Figure **S2** and Supplementary **Note 2**).

We first quantified the smFSH of Rhodamine B (RhB) featuring structurally rigid Xanthene core using this high-throughput SMS method. RhB molecules were deposited on glass substrates and imaged using sSMLM directly without additional sample preparation steps; camera exposure time is 50 ms for all smFSH measurements. Figure **2A** shows the averaged single-molecule emission spectrum measured from 11,734 single RhB molecules, where the emission maximum (λ_{Em}) is 578 nm, and the intensity-weighted spectral centroid (λ_{SC}) is 591 nm. The λ_{SC}, highlighted on the spectrum as a green circle, is commonly calculated in SMS to represent spectral signatures.[4,9,17] Figure **2B** shows 100 representative single-molecule emission spectra, which demonstrate the high smFSH of RhB. A photon count window (PCW, yellow dashed lines in Figures **2C**) between 500-1000 was applied and further used throughout all smFSH measurements for different types of fluorophores, allowing the systematic comparison of their smFSH at the same signal-to-noise level. A scatterplot of photon counts against λ_{SC} of the remaining 6,734 molecules depicts λ_{SC} varying from 560 nm to 660 nm with an extreme spread of about 100 nm (Figure **2C**). The mean photon count among all remaining molecules is 768, and the average spectral precision is 2.1 nm (Figure **S2B**). The observed high smFSH of RhB is consistent with our previous report of high smFSH in Tetramethyl Rhodamine (TAMRA).[5] Additionally, the histogram of λ_{SC} probability distribution shows a normal distribution (Figure **2D**, mean = 596 nm, standard deviation or STD = 9.2 nm). These results confirm that smFSH among different RhB molecules was captured by our high-throughput SMS. We then used the STD value of fluorophore's λ_{SC} probability distribution to quantify the extent of smFSH throughout the manuscript.

In comparison, we also characterized the smFSH of Alexa Fluor 647 (AF647), featuring structurally flexible polymethine bridges. We deposited AF647-IgG protein conjugates on glass substrates and imaged under a typical sSMLM imaging buffer[4, 9] to test AF647's smFSH at its widely used condition. Particularly, a scatterplot of photon count against λ_{SC} demonstrates their λ_{SC} varying only ~20 nm (from 680 nm to 700 nm, Figure **2E**). Additionally, the histogram of λ_{SC} probability distribution shows a relatively narrow distribution centered at 692 nm with an STD of 3.3 nm (Figure **2F**). This smFSH value is also consistent with the literature [4,9] and is 2.6-fold lower than that of RhB. We also measured the smFSHs of TAMRA-IgG (STD =9.0 nm) and AF647

directly deposited on glass (STD = 3.6 nm) as model systems to exclude environmental differences between the glass surfaces and IgG proteins (Figure **S3**). TAMRA has minimal structural differences from RhB (structures shown in Figures **S3A&B** insets); its λ_{SC} and STD values measured on the glass are very similar to those measured for RhB (Figure **S3A&B**). These values suggest that the observed differences of smFSH between Rhodamine derivatives and AF647 are pronounced at the same environment. Considering the structurally flexible polymethine bridges of AF647 and the relatively rigid Xanthene core of RhB (their molecular structures are shown in Figures **2E** and **2A**, respectively), AF647 possessing a significantly smaller smFSH, which is rather contradictory to the general perception that the more rigid molecule should have lower smFSH.

To understand this phenomenon and the cause of high smFSH in Rhodamines, we tested three potential sources that may lead to spectral variations and contribute to smFSH as hypothesized in Figure S**4**. First, we examined whether our smFSH measurement captures the snapshots of the spectral diffusion[24] from different RhB molecules while all RhB molecules possess the same high degree of spectral diffusion that is comparable with the observed smFSH (Figure **S4A**). Experimentally, we characterized the single-molecule spectral diffusion behaviors of 1,296 single RhB molecules imaged and then analyzed the statistics of their spectral diffusion behaviors. Second, we tested the influence of environment polarity changes on the spectral shifts in RhB (Figure **S4B**) using low-polarity polystyrene (PS)-coated glass substrates and Nile Red (NR) as a positive control. Third, we tested the hypothesis of co-existing conformational isomers in Rhodamines to cause spectral variations. We recently observed the co-existence of conformational isomers in Boron Dipyrromethene (BODIPY) chromophores, which caused spectral variations.[25] We measured the smFSH of Acridine Orange (AO), Rhodamine 101 (Rh101), a Perylene Diimide derivative (PDI), and Pentacene as model compounds to test our hypotheses (Figure **S4C**). Below we discussed the results related to the three potential causes of RhB's high smFSH and summarized the measured smFSH of different model fluorophores using different substrates in Table **1**. We also listed the relative polarity sensitivity and structural rigidity of model compounds in Table **2**.

First, we examined the spectral diffusion process, which has been observed frequently from single RhB molecules as a source of its smFSH. For each round of acquisition, we acquired 2,000 frames at an exposure time of 50 ms to monitor the single-molecule spectral diffusion behavior of

RhB. Figure **3A** plots the single-molecule emission spectral profiles of a representative RhB molecule over 63s. The spectral profiles remained relatively stable compared with the high spectral variations observed in Figure **4B** before the molecule photobleaches at the 63 s (or t_p = 63 s). The spectral and intensity trajectories of this RhB molecule are shown in Figure **3B** to quantify the spectral diffusion behavior. The intensity undergoes a single-step photobleaching process, which validated that our samples are at single-molecule density.[19] The λ_{SC} varies between 604-630 nm with an extreme spread of 26 nm. The histogram of λ_{SC} probability distribution of this RhB molecule during the 63-s emitting process (before bleaching) is shown in Figure **3C**, showing a relatively low STD of 3.3 nm. We then quantified the spectral diffusion process of 1,296 RhB molecules to examine the variations of spectral diffusion among different molecules (Figures **3D-3F**). Among all the characterized single RhB molecules, we found that the mean of STD, photon count, and t_p were 2.9 nm, 997 photons, and 5.7 s, respectively. We only found 8 out of 1296 molecules showed a spectral diffusion (STD > 9 nm) comparable to the observed smFSH of RhB. The mean STD measured from all the spectral diffusion processes was significantly lower than that observed for RhB. Therefore, the observed high smFSH of RhB is unlikely to be caused by the significant spectral variations in the single-molecule spectral diffusion process.

Second, we examined the effect of environmental polarity on smFSH in Rhodamines. Although environmental stimuli, such as polarity[26-27], pH[28-29], viscosity[30], temperature[31], and counter ion pairs [32] are reported to affect the fluorescence intensities of Rhodamines, their influences on spectral shifts are minor. For example, the averaged single-molecule spectra (λ_{SC} = 595 nm in PS) and smFSH of RhB (STD = 8.8 nm in PS) remained almost unchanged in low-polar PS-coated glass substrate (PS-RhB) compared with those measured in high-polar glass substrates (Glass-RhB) (Figures **4A & 4B**, and Table 1). The emission spectra of Rhodamines measured in low and high polar solvents (*i.e.,* Dichloromethane versus water) have only 15-nm shift[26,33]. In contrast, the polarity-sensitive NR showed 33-nm, and 1.7-nm differences in λ_{SC} and STD, respectively between PS substrate (PS-NR, λ_{SC} = 593 nm, STD = 6.1 nm) and glass substrates (Glass-NR, λ_{SC} = 616 nm, STD = 5.5 nm) (Figures **4C & 4D**, and Table 1). These results suggest that RhB is relatively insensitive to the environmental polarity changes compared to NR (see the relative polarity sensitivity scores in Table 2). Although the lactone form of Rhodamines emits at shorter wavelengths in a non-polar aprotic solvent, it cannot be efficiently excited and detected in

our setup[26]. Furthermore, our smFSH measurement was performed under neutral ambient conditions. Thus, the environmental change on the high smFSH of Rhodamine B is insignificant.

Third, we investigated whether conformational changes contribute to the smFSH of Rhodamines. The flexible dihedral angles between the Xanthene ring and the N, N-Dialkylated amino groups or between the Xanthene and the phenyl groups in RhB might cause the co-existence of multiple conformational isomers on glass surface which could possess distinct emission spectra that cause smFSH similar to what we observed in BODIPY chromophores[25]. To test these hypotheses, we measured the smFSH of AO and Rh101 as negative controls. AO shares a similar molecular structure with RhB except for a phenyl moiety and the Acridine core replacing the Xanthene core, which is used to examine the phenyl group's contribution to smFSH (Figure **5A**). Our smFSH measurement on AO demonstrates a broad λ_{SC} probability distribution with a mean of 561 nm and an STD of 9.0 nm (Figure **5B** and Table 1). The smFSH of AO is comparable with that of RhB, suggesting that removal of phenyl moiety does not reduce the smFSH. In principle, the rotamers caused by the rotation of the phenyl group will cause spectral changes because of drastically altered π-conjugation of the chromophore.[25] As we did not observe such a positive correlation between suppressed phenyl rotation and reduced the smFSH, we believe that the rotation of phenyl group of Rhodamine does not occur at our experimental condition. This result agrees with the literature report that the phenyl groups in Rhodamines are not in free rotation at room temperature.[34] In short, the phenyl group of Rhodamine is not in free rotation and does not contribute to the smFSH.

Similarly, we measured the smFSH of Rh101, whose flexible N, N-Dialkylated amino groups are interlocked by its fused six-member rings structure to the Xanthene core. Our measurement shows that Rh101 has a reduced smFSH of 6.7 nm, which is 2.5-nm smaller than RhB (mean λ_{SC} is 603 nm, Figures **5C &5D,** and Table 1), which indicates that the suppression of rotational flexibility in N, N-Dialkylated amino groups can reduce smFSH. We performed smFSH experiments on 5 different Rh101-Glass and RhB-Glass samples prepared and imaged under identical experimental conditions. We performed a statistical T-Test for the smFSH measurement between Rh101 and RhB results measured on the glass surface (Figure **S7**) and found that the P-value was less than 0.0001, indicating a statistical significance. Since λ_{SC} distributions of both RhB and Rh101 are normally distributed, and the rotational flexibility is independent of other sources

of smFSH origins, we calculated the contributions of this rotational flexibility to the smFSH according to probability theory[35]. The smFSH of Rhodamines caused by this conformational flexibility is 6.3 nm in STD or 47% in variances sSee the smFSH contribution section in the supporting information). Note that free rotation of N, N-Dialkylated amino groups of Rhodamines at room temperature is well-known with an activation energy of 6.6 kcal mol^{-1}.[34] A density functional theory (DFT) calculation indicates a consistently low activation energy (8.7 kcal mol^{-1}, Tables **S1-S2**) for this interconversion process in free solution.

We believe that such free rotations in solution will populate a broad distribution of the dihedral angles on the glass surface and result in the 2.5-nm increase in STD value for RhB compared with Rh101. We also performed time-dependent DFT (TDDFT) simulations to calculate λ_{Em} variations for RhB as a function of changing the dihedral angles of the N, N-Dialkylated amino groups (Figure **S8** and Table **S3**). The calculated λ_{Em} could vary at least 20 nm between 530 and 550 nm, which further supports our hypothesis that the co-existence of rotamers caused by the flexible N, N-Dialkylated amino groups can cause the smFSH (See more details in Supplementary Note 3). After adsorption to the glass surface, presumably, the interconversion of the rotamers significantly slows down or does not occur anymore upon RhB's interaction with the rigid glass surface. Otherwise, we would not observe a difference between the STD values of RhB and Rh101 using our 50 ms camera integration time; instead, we would observe a stable and broadened RhB emission spectrum because of the rapid interconversion among different camera frames. To clarify, we did not attempt to calculate the energies of the rotamers and simulate λ_{Em} probability based on a Boltzmann distribution because the detailed interactions and associated energy changes between the glass substrate and the Rhodamine molecules are challenging to simulate using existing glass models. In summary, the above results indicate that the N, N-Dialkylated amino group's rotational flexibility contributes significantly to the smFSH of RhB because of the co-existing of spectrally-distinct rotamers.

Although the rotamers can cause significant spectral variations, the remaining 6.7-nm smFSH observed in Rh101 must have additional sources. To exclude the rotational flexibility and test other possible sources of smFSH, we measured the smFSH of PDI and Pentacene, whose structures are extremely rigid with no rotational flexibilities (see their relative structural rigidity scores in Table 2). The histogram of λ_{SC} probability distributions of PDI is relatively broad, with an STD of 7.5

nm and a mean λ_{SC} of 622 nm (Figures **5E & 5F** and Table 1). Similarly, Pentacene's smFSH is also high, with an STD of 9.0 nm and a mean λ_{SC} of 601 nm (Figures **5G & 5H** and Table 1). Consistently, high smFSH of a relevant Rylene dye (Terylene Diimide, TDI) [36] has been reported with concomitant variations in both excitation spectra (STD = ~5.1 nm) and Stokes shifts (STD = ~3.4 nm) among different molecules. We believe that similar effects could also occur to Rhodamines. The reported variations of TDI's and other Rylene derivatives' excitation spectra indicate the heterogeneity of ground state energy among different molecules.[36-38] Besides, Pentacene samples measured on glass substrates show pronounced spectral shape changes and diminished fine emission peaks (*e.g.,* 0-1, 0-2 transitions) compared to the spectrum measured in solution (red and gray curves in Figure **5G**, respectively). This evidence implies that other uncommon nuclear coordinate changes (*e.g.,* structural deformations of the aromatic rings[39-40]) associated with heterogeneous environment[39] might also contribute to smFSH. The sampling of the ground state and excited state energy inhomogeneities by correlating experimental observations and simulations could shed light on the specific nuclear coordinate changes.

Lastly, the photooxidative N-dealkylations (often referred to as photobluing effect)[41] of Rhodamines can cause stepwise spectral shifts (~10-15 nm per step). In our spectral diffusion measurement of 1296 RhB molecules, we observed less than 10 distinct step-wise photobluing or photoredding events (examples shown in Figure **S5**). Further, we did not observe two additional peaks in the λ_{SC} histogram (Figure 2**D**) corresponding to the two sequential dealkylation steps. On the other hand, however, we measured the smFSH of Rhodamine 110 as a negative control, which is resistant to photobluing (Table **1** and Figure **S6**). It showed an STD value of 6.9 nm, which is 2.3-nm lower than that of RhB, and potentially indicates photobluing effect's potential contribution to the observed smFSH. Better model fluorophores and ultrafast single-molecule studies on the photobluing effect could help to understand the discrepancy between the two observations.

In conclusion, we developed a high-throughput method to capture $>5 \times 10^3$ single fluorescent molecules to investigate the observed high smFSH (STD = 9.2 nm) in RhB. To identify the causes of this smFSH, we quantified smFSHs from seven structurally relevant fluorophores deposited on glass and PS substrates. Using these model fluorophores and substrates of different polarities, we ruled out single-molecule spectral diffusion and environmental polarity changes as the primary

cause of smFSH. We found that the N, N-Dialkylated amino groups' rotational flexibility result in 2.5-nm increase in smFSH (STD value) and contribute 47% to the overall smFSH (variances value). With the observed high smFSH in structurally highly rigid fluorophores, we hypothesize that the remaining smFSH could arise from both Stokes shift variations and other uncommon nuclear coordinate changes. The fundamental understanding of such smFSH will guide the design of fluorophores with low smFSH for multiplexed sSMLM imaging and facilitate the interpretation of rich information using environment-sensitive probes for functional sSMLM imaging.

ASSOCIATED CONTENT

Supporting Information

The Supporting Information is available free of charge on the ACS Publications website at DOI: #.

Details on experimental setup, additional single-molecule and ensemble fluorescence spectral measurement, DFT/TDDFT calculation and supplementary notes on the imaging system's spectral precision measurement, achievable point density, and thermochemistry consideration.

AUTHOR INFORMATION

Corresponding Author

*yang.zhangfl@gmail.com

Author Contribution

[£]Yang Zhang and Yu Zhang contributed equally to this work.

Notes

The authors declare no competing financial interest.

ACKNOWLEDGMENT

The experimental work was supported in part by NSF grants CBET-1706642, EFMA-1830969, and CHE-1954430; and NIH grants R01GM140478, R01EY019949, and R01GM139151. GCS (theory work) was supported by DOE grant DE-SC0004752.

Reference

(1) Betzig, E.; Patterson, G. H.; Sougrat, R.; Lindwasser, O. W.; Olenych, S.; Bonifacino, J. S.; Davidson, M. W.; Lippincott-Schwartz, J.; Hess, H. F. Imaging Intracellular Fluorescent Proteins at Nanometer Resolution. *Science* **2006,** *313*, 1642.

(2) Rust, M. J.; Bates, M.; Zhuang, X. Sub-diffraction-limit imaging by stochastic optical reconstruction microscopy (STORM). *Nat. Methods* **2006,** *3,* 793-796.

(3) Jungmann, R.; Avendano, M. S.; Woehrstein, J. B.; Dai, M.; Shih, W. M.; Yin, P. Multiplexed 3D cellular super-resolution imaging with DNA-PAINT and Exchange-PAINT. *Nat. Methods* **2014,** *11*, 313-318.

(4) Zhang, Z.; Kenny, S. J.; Hauser, M.; Li, W.; Xu, K. Ultrahigh-throughput single-molecule spectroscopy and spectrally resolved super-resolution microscopy. *Nat. Methods* **2015,** *12*, 935-938.

(5) Dong, B.; Almassalha, L.; Urban, B. E.; Nguyen, T.-Q.; Khuon, S.; Chew, T.-L.; Backman, V.; Sun, C.; Zhang, H. F. Super-resolution spectroscopic microscopy via photon localization. *Nat. Commun.* **2016,** *7*, 12290.

(6) Huang, T.; Phelps, C.; Wang, J.; Lin, L. J.; Bittel, A.; Scott, Z.; Jacques, S.; Gibbs, S. L.; Gray, J. W.; Nan, X. *Simultaneous Multicolor Single-Molecule Tracking with Single-Laser Excitation via Spectral Imaging. Biophys. J.* **2018,** *114*, 301-310.

(7) Mlodzianoski, M. J.; Curthoys, N. M.; Gunewardene, M. S.; Carter, S.; Hess, S. T. uper-Resolution Imaging of Molecular Emission Spectra and Single Molecule Spectral Fluctuations. *PLoS ONE* **2016,** *11*, e0147506.

(8) Bongiovanni, M. N.; Godet, J.; Horrocks, M. H.; Tosatto, L.; Carr, A. R.; Wirthensohn, D. C.; Ranasinghe, R. T.; Lee, J.-E.; Ponjavic, A.; Fritz, J. V.; Dobson, C. M.; Klenerman, D.; Lee, S. F. Multi-dimensional super-resolution imaging enables surface hydrophobicity mapping. *Nat. Commun.* **2016,** *7*, 13544.

(9) Zhang, Y.; Song, K.-H.; Dong, B.; Davis, J. L.; Shao, G.; Sun, C.; Zhang, H. F. *Multicolor super-resolution imaging using spectroscopic single-molecule localization microscopy with optimal spectral dispersion. Appl. Opt.* **2019,** *58*, 2248-2255.

(10) Moon, S.; Yan, R.; Kenny, S. J.; Shyu, Y.; Xiang, L.; Li, W.; Xu, K. Spectrally Resolved, Functional Super-Resolution Microscopy Reveals Nanoscale Compositional Heterogeneity in Live-Cell Membranes. *J. Am. Chem. Soc.* **2017,** *139*, 10944-10947.

(11) Xiang, L.; Wojcik, M.; Kenny, S. J.; Yan, R.; Moon, S.; Li, W.; Xu, K. Optical characterization of surface adlayers and their compositional demixing at the nanoscale. *Nat. Commun.* **2018,** *9*, 1435.

(12) Davis, J.D..; Zhang, Y.; Yi, S.; Du, F.; Song, K.-H.; Scott, E. A.; Sun, C.; Zhang, H.F. Super-Resolution Imaging of Self-Assembled Nanocarriers Using Quantitative Spectroscopic Analysis for Cluster Extraction. *Langmuir* **2020**, *36*, 2291-2299.

(13) Zhanghao K.; Liu, W.; Li, M.; Wu, Z.; Wang, X.; Chen, X.; Shan, C.; Wang, H.; Chen, X.; Dai, Q.; Xi, P.; Jin, D. High-dimensional super-resolution imaging reveals heterogeneity and dynamics of subcellular lipid membranes. *Nat. Commun.* **2020**, *11*, 5890**.**

(14) Kim, D.; Zhang, Z.; Xu, K. Spectrally Resolved Super-Resolution Microscopy Unveils Multipath Reaction Pathways of Single Spiropyran Molecules. *J. Am. Chem. Soc.* **2017,** *139*, 9447-9450.

(15) Dong, B.; Soetikno, B. T.; Chen, X.; Backman, V.; Sun, C.; Zhang, H. F. Parallel Three-Dimensional Tracking of Quantum Rods Using Polarization-Sensitive Spectroscopic Photon Localization Microscopy. *ACS Photonics* **2017,** *4*, 1747-1752.

(16) Upadhyayula, S.; Nunez, V.; Espinoza, E. M.; Larsen, J. M.; Bao, D.; Shi, D.; Mac, J. T.; Anvari, B.; Vullev, V. I. Photoinduced dynamics of a cyanine dye: parallel pathways of non-radiative deactivation involving multiple excited-state twisted transients. *Chem. Sci.* **2015,** *6*, 2237-2251.

(17) Lu, H. P.; Xie, X. S. Single-molecule spectral fluctuations at room temperature. *Nature* **1997,** *385*, 143-146.

(18) Wazawa, T.; Ishii, Y.; Funatsu, T.; Yanagida, T. Spectral fluctuation of a single fluorophore conjugated to a protein molecule. *Biophys. J.,* **2000,** *78*, 1561-1569.

(19) Ha, T.; Enderle, T.; Ogletree, D. F.; Chemla, D. S.; Selvin, P. R.; Weiss, S. Probing the interaction between two single molecules: fluorescence resonance energy transfer between a single donor and a single acceptor. *Proc. Natl. Acad. Sci.,* **1996,** *93*, 6264-6268.

(20) Empedocles, S. A.; Neuhauser, R.; Shimizu, K.; Bawendi, M. G. Photoluminescence from Single Semiconductor Nanostructures. *Adv. Mater.* **1999**, 11, 1243-1256.

(21) Empedocles, S. A.; Norris, D. J.; Bawendi, M. G. Photoluminescence Spectroscopy of Single CdSe Nanocrystallite Quantum Dots. *Phys. Rev. Lett.* **1996**, 77, 3873-3876

(22) Song, K.-H.; Dong, B.; Sun, C.; Zhang, H. F. Theoretical analysis of spectral precision in spectroscopic single-molecule localization microscopy. *Rev. Sci. Instrum.* **2018,** 89, 123703

(23) Silverman, B.W., *Density Estimation for Statistics and Data Analysis*; CRC Press, **1986**

(24) Ambrose, W.P.; Moerner, W. E. Fluorescence spectroscopy and spectral diffusion of single impurity molecules in a crystal. *Nature* **1991**, *349*, 225-227.

(25) Sansalone, L.; Zhang, Y.; Mazza, M. M. A.; Davis, J.; Song, K. H.; Captain, B.; Zhang, H. F.; Raymo, F. M. High-Throughput Single-Molecule Spectroscopy Resolves the Conformational Isomers of BODIPY Chromophores. *J. Phys. Chem. Lett.* **2019**, 10, 6807-6812.

(26) Beija, M.; Afonso, C. A.; Martinho, J. M. Synthesis and applications of Rhodamine derivatives as fluorescent probes. *Chem. Soc. Rev.* **2009,** *38*, 2410-33.

(27) Jadhav, A. G.; Kothavale, S.; Sekar, N. Red emitting triphenylamine based rhodamine analogous with enhanced Stokes shift and viscosity sensitive emission. *Dyes Pigm.* **2017,** *138*, 56-67.

(28) Macdonald, P. J.; Gayda, S.; Haack, R. A.; Ruan, Q.; Himmelsbach, R. J.; Tetin, S. Y. Rhodamine-Derived Fluorescent Dye with Inherent Blinking Behavior for Super-Resolution Imaging. *Anal. Chem.* **2018,** *90*, 9165-9173.

(29) Stratton, S. G.; Taumoefolau, G. H.; Purnell, G. E.; Rasooly, M.; Czaplyski, W. L.; Harbron, E. J. Tuning the pKa of Fluorescent Rhodamine pH Probes through Substituent Effects. *Chem. Eur. J.* **2017,** *23,* 14064-14072.

(30) Tredwell, C. J.; Osborne, A. D. Viscosity dependent internal conversion in the rhodamine dye, fast acid violet 2R. *J. Chem. Soc., Faraday Trans. 2* **1980,** *76*, 1627-1637.

(31) Soleilhac, A.; Girod, M.; Dugourd, P.; Burdin, B.; Parvole, J.; Dugas, P. Y.; Bayard, F.; Lacote, E.; Bourgeat-Lami, E.; Antoine, R. Temperature Response of Rhodamine B-Doped Latex Particles. From Solution to Single Particles. *Langmuir* **2016,** *32*, 4052-4058.

(32) Köhn, F.; Hofkens, J.; De Schryver, F. C. Emission of the contact ion pair of rhodamine dyes observed by single molecule spectroscopy. *Chem. Phys. Lett.* **2000,** *321*, 372-378.

(33) Nag, A.; Goswami, D. Solvent effect on two-photon absorption and fluorescence of rhodamine dyes. *J. Photochem. Photobiol. A* **2009,** *206,* 188-197.

(34) Karstens, T.; Kobs, K. Rhodamine B and rhodamine 101 as reference substances for fluorescence quantum yield measurements. *J. Phys. Chem.* **1980,** *84*, 1871-1872.

(35) Lmons, D. S. *An Introduction to Stochastic Processes in Physics.* Johns Hopkins University Press, **2002**

(36) Thyrhaug, E.; Krause, S.; Perri, A.; Cerullo, G.; Polli, D.; Vosch, T.; Hauer, J. Single-molecule excitation–emission spectroscopy. *Proc. Natl. Acad. Sci.* **2019,** 116, 4064-4069.

(37) Stopel, M. H.; Blum, C.; Subramaniam, V. Excitation Spectra and Stokes Shift Measurements of Single Organic Dyes at Room Temperature. *J. Phys. Chem. Lett.* **2014,** *5*, 3259-64.

(38) Piatkowski, L.; Gellings, E.; van Hulst, N. F. Broadband single-molecule excitation spectroscopy. *Nat. Commun.* **2016,** *7*, 10411.

(39) Kemnitz, K.; Tamai, N.; Yamazaki, I.; Nakashima, N.; Yoshihara, K. Site-dependent fluorescence lifetimes of isolated dye molecules adsorbed on organic single crystals and other substrates. *J. Phys. Chem.* **1987,** *91*, 1423-1430.

(40) Hofkens, J.; Vosch, T.; Maus, M.; Köhn, F.; Cotlet, M.; Weil, T.;Herrmann, A.; Müllen, K.; De Schryver, F. C. Conformational rearrangements in and twisting of a single molecule. *Chem. Phys Lett.* **2001,** *333,* 255-263.

(41) Butkevich, A. N.; Bossi, M. L.; Lukinavicius, G.; Hell, S. W. Triarylmethane Fluorophores Resistant to Oxidative Photobluing. *J. Am. Chem. Soc.* **2019,** *141*, 981-989.

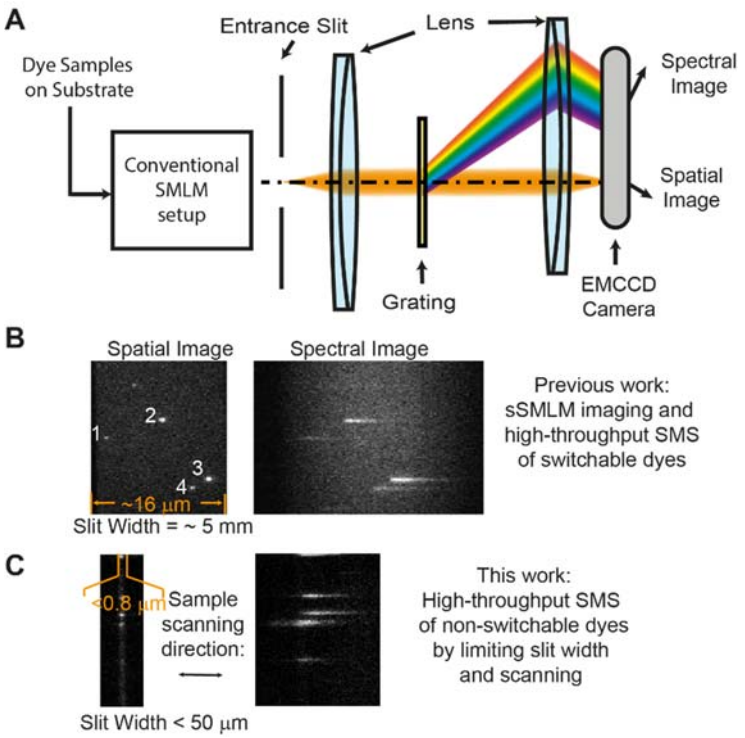

Figure 1. (**A**) Schematic of the sSMLM system; (**B**) Example spatial and spectral images in sSMLM, showing the spatial locations and their corresponding emission spectra of four individual single-molecules (highlighted by 1-4); (**C**) New high-throughput SMS of non-switchable fluorophores were obtained by acquiring the high-density single-molecule sample and scanning the sample stage, where the slit width was < 80 μm to provide narrow spatial images (FOV's width < 0.8 μm). As a result, only the spectral images of the single molecules within this narrow FOV can be captured.

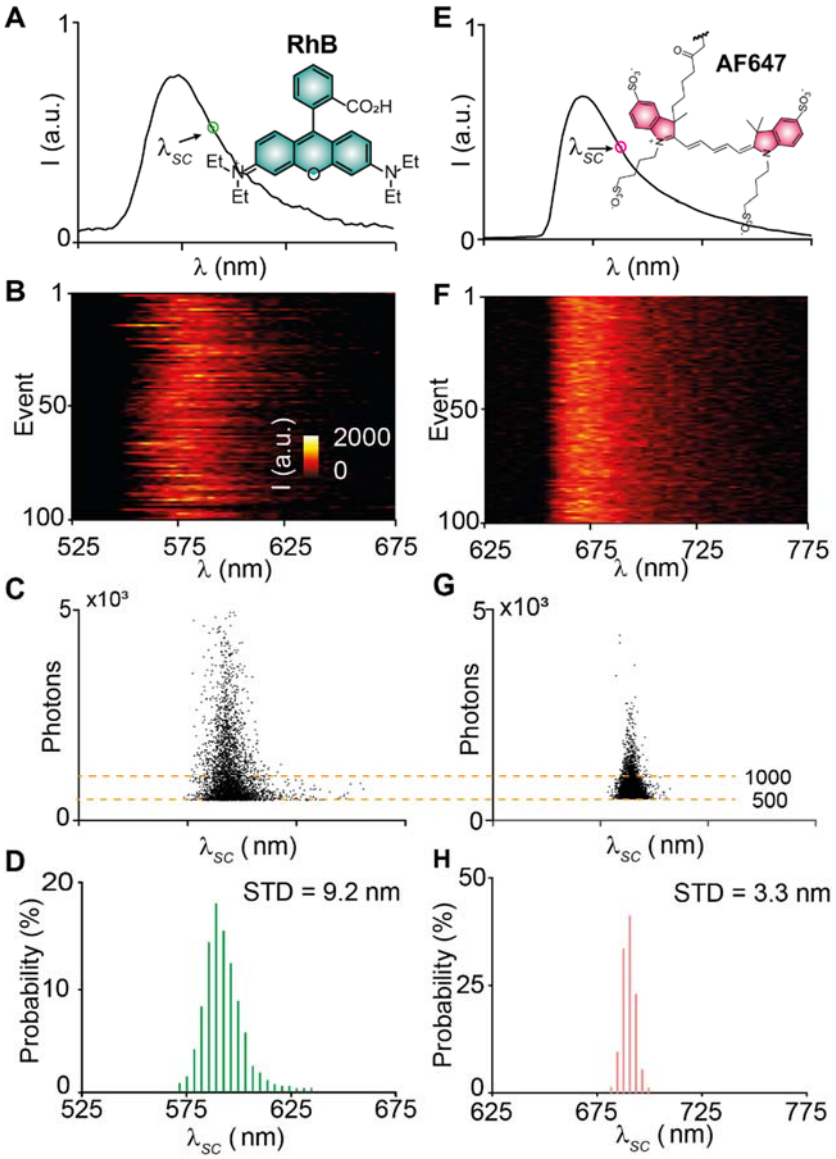

Figure 2. Measured smFSH properties of RhB (**A**-**D**) and AF647 (**E**-**H**). (**A**) Averaged single-molecule emission spectra of RhB deposited on glass substrate obtained from 11, 734 single RhB molecules. The green circle highlights the λ_{SC} position. The structure of RhB is shown in the inset; (**B**) 100 representative single-molecule emission spectra of RhB; (**C**) Scatterplot of photon counts against λ_{SC} from all the RhB molecules; a PCW (indicated by the yellow dashed lines) of 500-1000 photons was applied to compare smFSH at the same signal level for different types of fluorophores; (**D**) Histogram of the probability distribution of λ_{SC} from the remaining 6,734 RhB molecules; **(E)** Averaged single-molecule emission spectra of AF647-IgG protein conjugate deposited on glass substrate obtained from 5,376 single AF647 molecules. The red circle highlights the λ_{SC} position. The structure of AF647 is shown in the inset; (**F**) 100 representative single-molecule emission spectra of AF647; (**C**) Scatterplot of photon counts against λ_{SC} from all the AF647 molecules; the same PR was applied to analyze smFSH; (**H**) histogram of the probability distribution of λ_{SC} for the remaining 2,763 AF647 single molecules.

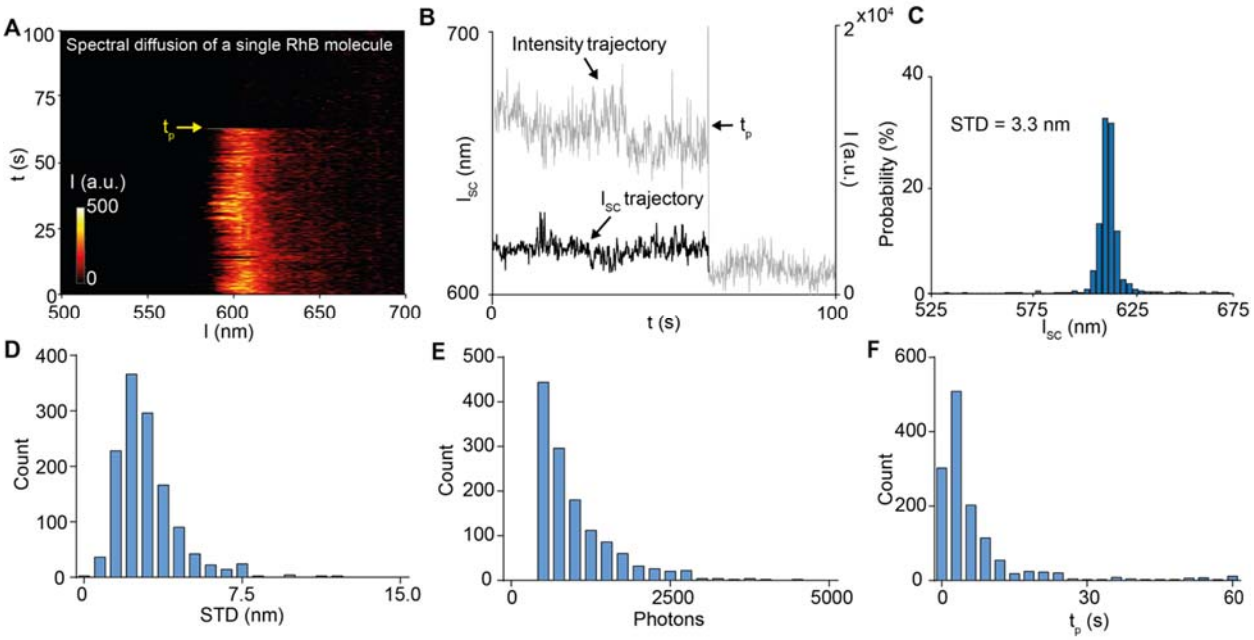

Figure 3. Single-molecule spectral diffusion behaviors and statistical analyses of single RhB molecules. (**A**) The single-molecule spectra of a representative RhB molecule imaged for 62 s; (**B**) Single-molecule λ_{SC} and intensity-trajectories of this RhB molecule; t_p indicates the time of photobleaching; (**C**) Histogram of λ_{SC} distribution of this RhB molecule over the entire acquisition process before photobleaching; The histograms of STD (**D**), averaged photon numbers (**E**), and t_p (**F**) distributions from 1,296 single molecules.

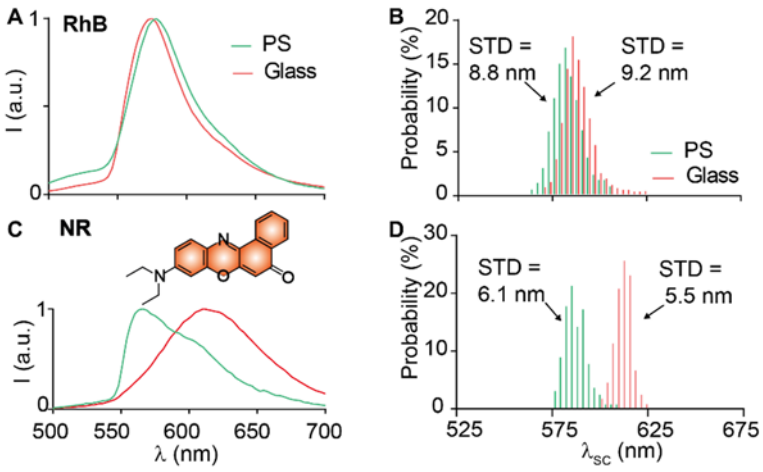

Figure 4. Characterizing smFSH properties of RhB (**A**-**B**) and NR (**C**-**D**), on different substrates. (**A** and **C**) Averaged single-molecule emission spectra of RhB and Nile Red deposited on glass (red curve) and PS (green curve) substrates, respectively; (**B** and **D**) Histogram of probability distributions for RhB and NR deposited on glass (red bars) and PS (green bars), respectively.

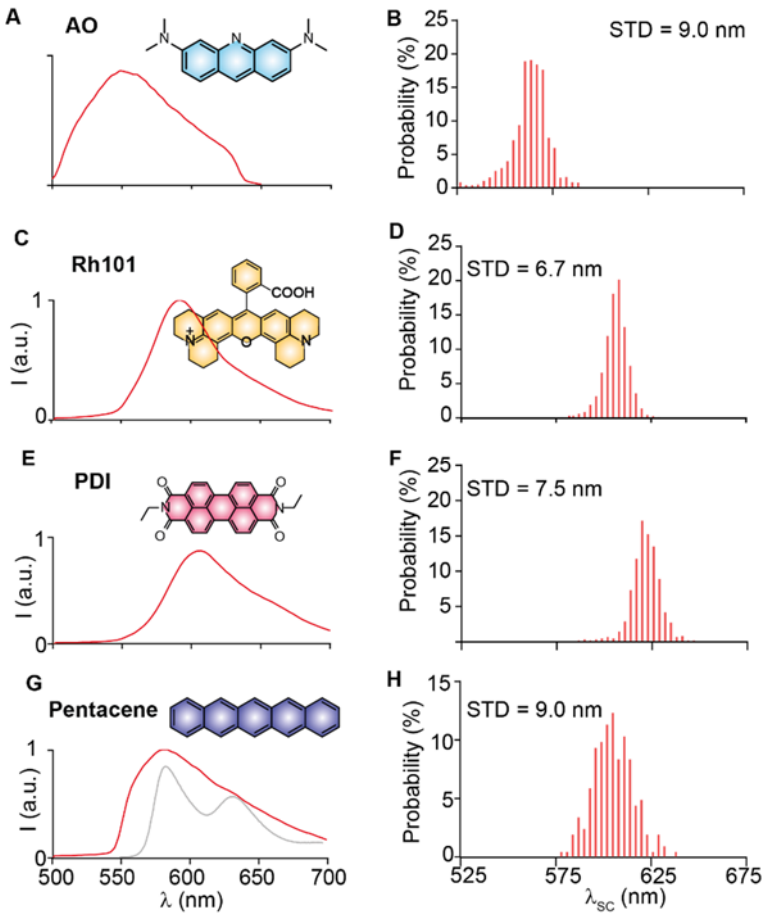

Figure 5. Characterizations smFSH properties of AO (**A**-**B**), Rh101 (**C**-**D**), PDI (**E**-**F**), and Pentacene (**G**-**H**) on glass substrates. (**A**, **C**, **E**, **G**) Averaged single-molecule emission spectra of AO, Rh101, PDI and Pentacene deposited on glass substrates, respectively; (**B**, **D**, **F**, **H**) Histogram of probability distributions for AO, Rh101, and Pentacene deposited on glass substrates, respectively.

Table 1. Averaged single-molecule λ_{SC} and STD of λ_{SC} probability distribution of RhB, AF647, TAMRA, AO, Nile Red, Rh101, Rh110, PDI, and Pentacene on different substrates at 25 °C

	λ_{SC} (nm) [a]	STD (nm)
IgG-AF647	690	3.3
Glass-AF647	688	3.6
Glass-RhB	596	9.2
Glass-TAMRA	591	8.8
IgG-TAMRA	596	9.0
PS-RhB	595	8.8
Glass-NR	616	5.5
PS-NR	593	6.1
Glass-AO	561	9.0
Glass-Rh101	603	6.7
Glass-PDI	622	7.5
Glass-Pentacene	601	9.0
Glass-Rh110	553	6.9

[a] λ_{SC} measured from the averaged single-molecule emission spectra.

Table 2. The relative polarity-sensitivity and structural rigidity of RhB, NR, AO, Rh101, PDI, and Pentacene

	Polarity Sensitivity	Structural Rigidity
RhB	-	-
NR	+	N/A
AO	N/A	+
Rh101	-	+
PDI	-	++
Pentacene	-	++

++: Extremely high; +: high; -: low; N/A: non-applicable